PAPER

Check for updates

LiBa$_3$Al$_2$B$_3$O$_{11}$: a deep-ultraviolet transparent optical borate featuring a 2D [Al$_2$B$_3$O$_{11}$]$_\infty$ layered structure

Shuangyue Shang, [ID] [a,b] Fan Liu, [a,b] Lei Kang, [ID] [a] Tong Wu, [ID] [a,b] Tianhong Huang, [a,b] Lijuan Liu*[a] and Xiaoyang Wang [ID] *[a]

Borates have garnered significant attention due to their rich structural diversity and versatile applications, particularly in the ultraviolet (UV) and deep-ultraviolet (DUV) transparent optical regions. In this study, a new aluminum borate, LiBa$_3$Al$_2$B$_3$O$_{11}$, was successfully synthesized for the first time. Its structural framework consists of interconnected [BO$_3$]$^{3-}$ triangles and [Al$_2$O$_6$]$_\infty$ chains, with Ba and Li atoms occupying the interstitial sites. Within the a–c plane, the crystal features two-dimensional [Al$_2$B$_3$O$_{11}$]$_\infty$ layers composed of 16-membered rings (Al$_2$B$_2$O$_6$), which remains a unique structure motif among aluminum borates. Experimental results confirmed a UV transmission cut-off edge below 200 nm, indicating its potential for applications in DUV optics.

Introduction

Borates have long been recognized as promising candidates for applications in the ultraviolet (UV) and deep-ultraviolet (DUV) transparent regions due to their rich structural diversity.[1–5] The borate (B$_x$O$_y$) system is characterized by a variety of fundamental building units, primarily the trigonal planar [BO$_3$]$^{3-}$ and the tetrahedral [BO$_4$]$^{5-}$ groups.[6–9] These basic units can further link together to form more complex groups, such as the [B$_3$O$_6$]$^{3-}$ ring in β-BaB$_2$O$_4$ (β-BBO) and the [B$_3$O$_7$]$^{5-}$ ring in LiB$_3$O$_5$ (LBO).[10,11] Moreover, these borate groups can interconnect with polyhedral structural units centered on elements like Be, Al, Zn, Ga or Si to build the overall framework of the compound.[12–19] These structurally diverse borates have shown great potential for applications in self-frequency-doubling crystals, birefringent materials, and nonlinear optics.[20–23]

In recent years, the Al–B–O system has garnered significant attention and extensive research.[24–28] A series of notable nonlinear optical (NLO) crystals, such as K$_2$Al$_2$B$_2$O$_7$ (KABO) and Cs$_2$(AlB$_3$O$_6$)$_2$O, have been discovered based on structural analogues Sr$_2$Be$_2$B$_2$O$_7$ (SBBO).[29,30] Furthermore, the exploration of aluminum borates with novel structures is ongoing. For instance, Ca$_3$Al$_2$B$_8$O$_{18}$ was reported in 2024, featuring a framework composed of [B$_6$O$_{16}$]$_\infty$ chains connected by isolated [AlO$_4$]$^{5-}$ groups.[31] The three-dimensional [Al$_4$B$_4$O$_{10}$] skeleton of BaAlBO$_4$, reported in 2019, was constructed from [Al$_4$O$_{10}$]$_\infty$ layers bridged by isolated [B$_4$O$_{10}$]$^{8-}$ groups.[32] The framework of Li$_2$AlBO$_4$ consists of [Al$_2$O$_6$]$_\infty$ chains connected by isolated [BO$_3$]$^{3-}$ groups.[33] The primary building units in aluminum borate structures include isolated Al–O groups such as [AlO$_4$]$^{5-}$, [AlO$_6$]$^{9-}$, and [Al$_2$O$_7$]$^{8-}$, as well as Al–O chains. Among aluminum borates, Li$_2$AlBO$_4$ and KSrAl$_3$B$_2$O$_9$ are known rare aluminum borates, whose anionic framework comprises isolated [BO$_3$]$^{3-}$ units and [Al$_2$O$_6$]$_\infty$ chains. These studies significantly enrich the structural diversity of the aluminum borate system and demonstrate its great potential.

In pursuit of novel aluminum borates with specific structural motifs for DUV transparent applications, we strategically targeted compounds within the Li–Ba–Al–B–O system. This approach led to the successful synthesis of a new aluminum borate, LiBa$_3$Al$_2$B$_3$O$_{11}$. Its structure is composed of [BO$_3$]$^{3-}$ planar triangles coordinated with [Al$_2$O$_6$]$_\infty$ chains, forming a novel two-dimensional [Al$_2$B$_3$O$_{11}$]$_\infty$ layered framework. To the best of our knowledge, this structure motif has not been previously reported. The compound exhibits an optical cutoff edge below 200 nm, indicating its potential for DUV transparent applications. This paper presented the crystal structure of LiBa$_3$Al$_2$B$_3$O$_{11}$, along with details of its synthesis, optical properties, and thermal analysis. Additionally, the electronic structure and refractive index of the title compound were calculated.

Experimental section

Synthesis and crystal growth

Polycrystalline LiBa$_3$Al$_2$B$_3$O$_{11}$ samples were synthesized *via* the solid-state reaction method. High-purity BaCO$_3$, Li$_2$CO$_3$, Al$_2$O$_3$,

[a]*Beijing Center for Crystal Research and Development, Technical Institute of Physics and Chemistry (TIPC), Chinese Academy of Sciences, Beijing 100190, China. E-mail: xywang@mail.ipc.ac.cn, llj@mail.ipc.ac.cn*
[b]*University of Chinese Academy of Science, Beijing 100049, China*

and H_3BO_3 were weighed in a molar ratio of $6:1:2:6$ and thoroughly ground into a homogeneous mixture. The powders were then loaded into a platinum crucible. To ensure complete homogenization, the mixture was several times gradually heated to 700 °C in a resistive-heating furnace, removed, and reground. The formation of a pure $LiBa_3Al_2B_3O_{11}$ phase was confirmed *via* powder X-ray diffraction (PXRD) analysis. Single crystals of $LiBa_3Al_2B_3O_{11}$ were grown using the melt-growth method. The polycrystalline powder, prepared as described above, was gradually heated to 900 °C and held for 24 hours to ensure complete melting. The melt was then cooled to 700 °C at a rate of 2 °C h^{-1} and then rapidly cooled to room temperature. After the growth process, the single crystals were obtained.

Structure determination and PXRD

Single-crystal XRD data were measured at room temperature on a Bruker D8 Quest diffractometer equipped with a Mo Kα radiation source ($\lambda = 0.71073$ Å). The crystal structure was solved and refined by the SHELXL program. The PXRD pattern of the experimental sample was recorded on a Bruker D8 diffractometer using Cu Kα radiation. The measurement parameters were as follows: a 2θ range of 5° to 70°, a step size of 0.02°, and a counting time of 0.1 s per step.

Elemental analysis

Elemental analysis was performed using an energy dispersive spectroscopy (EDS, OXFORD X-MaxN 80) equipped with a field-emission scanning electron microscope (SEM, QUANTA FEG 250).

Thermal analysis

The thermal properties of $LiBa_3Al_2B_3O_{11}$ crystals were investigated using a NETZSCH STA 409 CD simultaneous thermal analyzer. A 13.634 mg crystal powder, placed in a platinum crucible at room temperature, was heated from room temperature to 1200 °C at a rate of 10 K min^{-1}, and then cooled to 80 °C at 10 K min^{-1} under an atmosphere of nitrogen.

Optical spectroscopy

The UV-Vis transmittance spectrum of $LiBa_3Al_2B_3O_{11}$ was measured using an Agilent Cary 7000 spectrophotometer in the wavelength range of 200 to 1200 nm, with polytetrafluoroethylene used as a reference standard. The infrared (IR) spectroscopy of $LiBa_3Al_2B_3O_{11}$ was measured at room temperature using a Fourier Transform Infrared Spectrometer (Excalibur 3100) in the range of 400 to 2000 cm^{-1}. The dried $LiBa_3Al_2B_3O_{11}$ and KBr powders were mixed in a mass ratio of $1:100$ and then pressed into sheets.

Theoretical calculations

First-principles calculations based on the density functional theory (DFT) were carried out on $LiBa_3Al_2B_3O_{11}$ using the plane-wave pseudopotential method implemented in the CASTEP package to explore its electronic structure.[34,35] The Perdew–Bruke–Ernzerhof (PBE) functional under generalized gradient approximation (GGA) was chosen for the exchange–correlation functional.[36] Ultrasoft pseudopotentials were used for all elements. The structural parameters were based on experimental data, and no structure optimization was performed during the calculations. For $LiBa_3Al_2B_3O_{11}$, the plane wave cut-off energy and Monkhorst–Pack k point grid in the Brillouin zone were set at 340 eV and $4 \times 1 \times 3$, respectively. The band structure, refractive index, and partial density of states (PDOS) were calculated to elucidate the structure–property relationship of $LiBa_3Al_2B_3O_{11}$. Owing to the underestimation of bandgap by GGA functional, the screened exchange PEB0 functional was used to calculate the bandgap in high accuracy.[37]

Results and discussion

Crystal structure

The crystallographic data and structure refinement parameters were summarized in Table 1. $LiBa_3Al_2B_3O_{11}$ crystallizes in the triclinic crystal system with the $P2_1/c$ (14) space group. The unit cell parameters are $a = 6.5729(3)$, $b = 17.5252(7)$, $c = 9.6851(4)$, $\alpha = \gamma = 90°$, $\beta = 100.6530(10)°$, and $Z = 4$. The asymmetric unit contains three Ba atoms, one Li atom, two Al atoms, three B atoms, and eleven O atoms. The structure comprises five distinct structural groups: $[AlO_4]^{5-}$ tetrahedron, $[BO_3]^{3-}$ planar triangle, $[LiO_4]^{7-}$ distorted tetrahedron, and Ba-centered $[BaO_8]^{14-}$ and $[BaO_{10}]^{18-}$ polyhedra. The coordination environments of B, Al, Li, and Ba atoms are depicted in Fig. 1(a)–(e).

As shown in Fig. 2(a), $[AlO_4]^{5-}$ tetrahedra are interconnected *via* shared oxygen atoms to form $[Al_2O_6]_\infty$ chains,

Table 1 Crystal data and structural refinement of $LiBa_3Al_2B_3O_{11}$

|	
Formula	$LiBa_3Al_2B_3O_{11}$
Formula weight	681.35
Temperature/K	296.15
Crystal system	Monoclinic
Space group	$P2_1/c$
a/Å	6.5729(3)
b/Å	17.5252(7)
c/Å	9.6851(4)
α/°	90
β/°	100.6530(10)
γ/°	90
Volume/Å^3	1096.41(8)
Z	4
ρ_{calc}g/cm^3	4.128
μ/mm^{-1}	10.867
$F(000)$	1200.0
Radiation	Mo Kα ($\lambda = 0.71073$)
2θ range for data collection/°	4.87 to 66.334
Index ranges	$-8 \leq h \leq 10, -26 \leq k \leq 26, -14 \leq l \leq 14$
Reflections collected	17 360
Independent reflections	4164 [$R_{int} = 0.0647$, $R_{sigma} = 0.0668$]
Data/restraints/parameters	4164/0/182
Goodness-of-fit on $F2$	1.078
Final R indexes [$I \geq 2\sigma(I)$]	$R_1 = 0.0411$, w$R_2 = 0.0643$
Final R indexes [all data]	$R_1 = 0.0665$, w$R_2 = 0.0732$
Largest diff. peak/hole/e Å^{-3}	1.60/−1.71
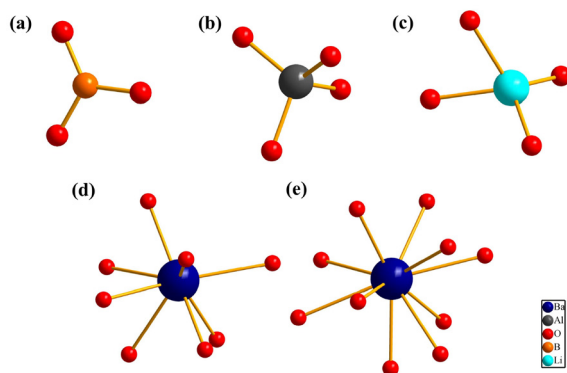
Fig. 1 The atomic coordination environments. (a) B atoms, (b) Al atoms, (c) Li atoms, (d) and (e) Ba atoms.

which are further bridged by $[BO_3]^{3-}$ planar triangles. In addition, each $[AlO_4]^{5-}$ group is connected to a dangling $[BO_3]^{3-}$ group through a shared oxygen atom, forming a two-dimensional $[Al_2B_3O_{11}]_\infty$ layer in the a–c plane. These layers contain 16-membered rings $(Al_2B_2O_6)$, as illustrated in Fig. 2(b). The arrangement of $[BO_3]^{3-}$ groups in the unit cell along the b axis is demonstrated in Fig. 2(c), where $[BO_3]^{3-}$ are not coplanar. Fig. 2(d) displays the Ba–O coordination network with three coordination modes. The blue-marked polyhedra in the figure correspond to a ten-coordination Ba site. In Fig. 2(e), the two-dimensional $[Al_2B_3O_{11}]_\infty$ layer alternates with Ba atoms, dangling $[BO_3]^{3-}$, and Li atoms along the b axis. The Ba atoms are embedded within the layers, and Li atoms are positioned interstitially between the layers to maintain a charge balance. The interlayer distance is 8.7626 Å. The single-layer crystal structure observed on the a–c plane is shown in

Fig. 2(f). The atomic coordinates and equivalent isotropic displacement parameters (Å^2), anisotropic displacement parameters (Å^2), bond lengths (Å), bond angles (degrees), and torsion angles for $LiBa_3Al_2B_3O_{11}$ are listed in Tables S1–S5. The results of bond valence (BVS) calculations (Li: 1.085, Ba: 1.890–2.067, Al: 3.088–3.133, B: 2.930–2.947, and O: 1.682–2.158) showed that the oxidation states of Li, Ba, Al, B, and O atoms were +1, +2, +3, +3, −2, respectively. This result was consistent with the single-crystal structure analysis.

Optical properties

The UV-Vis spectrum of $LiBa_3Al_2B_3O_{11}$ was measured, as shown in Fig. 3(a), revealing a transmittance of approximately 88% in the visible light region. Below 450 nm, the transmittance decreases due to extrinsic absorption, reaching a residual value of 33.08% at 200 nm. This result indicates that the cut-off wavelength of the $LiBa_3Al_2B_3O_{11}$ is below 200 nm, highlighting its potential in the DUV transparent region. The IR spectrum of $LiBa_3Al_2B_3O_{11}$ is presented in Fig. 3(b). The absorption peaks from 1400 to 1247 cm^{-1} are attributed to the
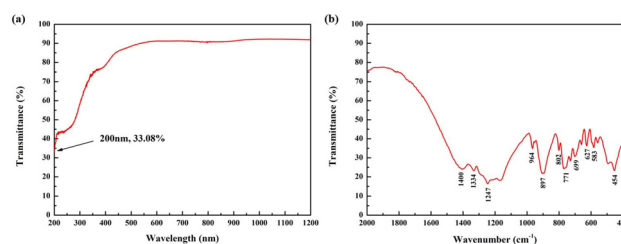

Fig. 3 Optical spectra. (a) UV-Vis transmittance spectrum of $LiBa_3Al_2B_3O_{11}$, (b) IR spectrum.

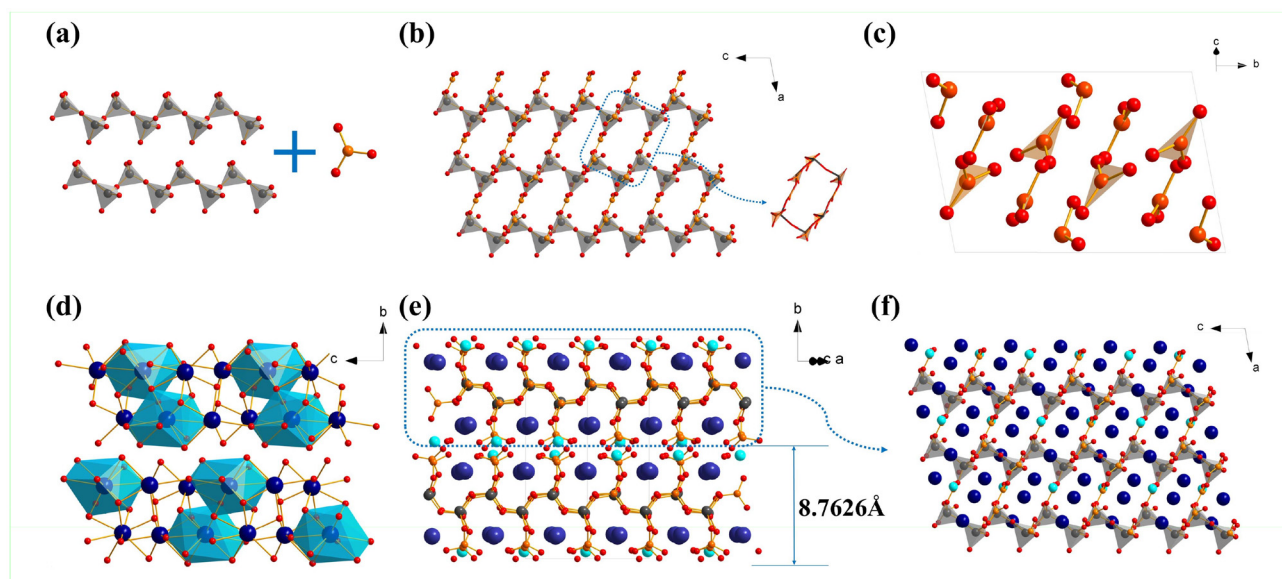**Fig. 2** Crystal structure of $LiBa_3Al_2B_3O_{11}$. (a) $[Al_2O_6]_\infty$ chains, (b) two-dimensional $[Al_2B_3O_{11}]_\infty$ layer, (c) arrangement of $[BO_3]^{3-}$ groups along the a–c plane, (d) Ba–O coordination network, (e) crystal structure along the b axis, (f) single-layer structure observed on the a–c plane.

asymmetric stretching vibrations of $[BO_3]^{3-}$ group, and the peaks between 964 and 802 cm^{-1} are attributed to its symmetric stretching vibration.[32,38–40] The peaks of bending vibrations of the $[BO_3]^{3-}$ group are located from 771 to 627 cm^{-1}, while those below 600 cm^{-1} are associated with the overlapping vibrations of B–O and Al–O bonds.[41–43]

Elemental composition analysis and XRD

The elemental composition of $LiBa_3Al_2B_3O_{11}$ is analyzed, as shown in Fig. S1. The EDS result reveals that the molar ratio of Ba, Al, and O is approximately $3:2:11$, aligning with the single-crystal refinement data. However, the detection of B and Li elements is unreliable in EDS analysis due to their low atomic numbers and limited sensitivity of the technique. Fig. 4(a) displays the XRD patterns of the crystals (red line) and the polycrystalline powder (blue line), both of which agree well with the single-crystal simulated XRD pattern (black line).

Thermal behavior analysis

Fig. 4(b) presents the results of the Differential Scanning Calorimetry (DSC) and Thermogravimetric (TG) for $LiBa_3Al_2B_3O_{11}$. An endothermic peak at 806 °C corresponds to the melting of $LiBa_3Al_2B_3O_{11}$. Upon cooling, crystallization occurs with a ~146 °C undercooling, as indicated by a weak exotherm at 660 °C, which is attributed to the high viscosity of the melt. As displayed in the above XRD patterns, the samples of $LiBa_3Al_2B_3O_{11}$ before and after melting are nearly identical, suggesting that it is a congruently melting compound. The TG curve demonstrates no mass loss during both heating and cooling processes.

Calculation results

The band structure of $LiBa_3Al_2B_3O_{11}$ crystal was determined by the first-principles calculations. As shown in Fig. 5(a), the valence band maximum and the conduction band minimum of $LiBa_3Al_2B_3O_{11}$ are located at the same position (G point in the Brillouin zone). Therefore, $LiBa_3Al_2B_3O_{11}$ is a direct bandgap compound with a calculated bandgap of 5.64 eV. The calculated partial density of states (PDOS) of $LiBa_3Al_2B_3O_{11}$ is shown in Fig. 5(b). The upper part of the valence band is mainly composed of 2p orbitals, and there is significant overlap between the B 2p and 2p orbitals. The bottom part of the conduction band is contributed by the orbitals of all
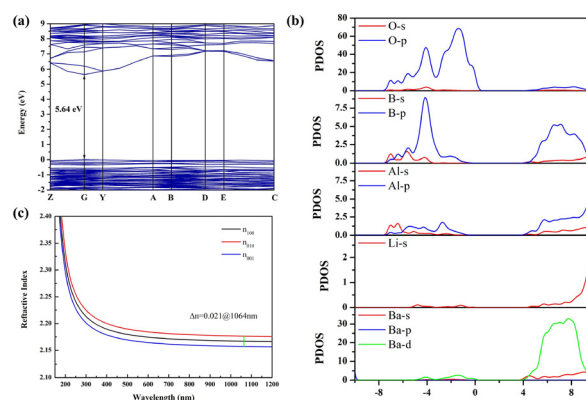

Fig. 5 Calculated (a) band structure, (b) partial density of states, (c) refractive index of $LiBa_3Al_2B_3O_{11}$.

atoms. This indicates that the $[BO_3]^{3-}$ building units contribute significantly to the optical properties of $LiBa_3Al_2B_3O_{11}$. The calculated refractive index is presented in Fig. 5(c) with $\Delta n = 0.021$ at 1064 nm. As shown in Fig. 2, the $[BO_3]^{3-}$ groups in $LiBa_3Al_2B_3O_{11}$ are isolated and interconnected with $[AlO_4]^{5-}$ unit *via* shared oxygen atoms. The connectivity forms a layered structure that reduces dangling oxygen atoms and contributes to an enlarged band gap. For birefringence, the $[BO_3]^{3-}$ groups exhibit a non-coplanar arrangement with disordered interlayer stacking. This configuration diminishes the net optical anisotropy, resulting in a small birefringence.

Conclusions

In summary, a new deep-ultraviolet transparent borate, $LiBa_3Al_2B_3O_{11}$, was discovered in the Li–Ba–Al–B–O system under open conditions. The compound features a two-dimensional $[Al_2B_3O_{11}]_\infty$ layer framework composed of $[BO_3]^{3-}$ groups and $[Al_2O_6]_\infty$ chains. The research demonstrates that this compound exhibits a UV cut-off edge below 200 nm. Targeted structural modifications, such as the introduction of polar atoms or the optimization of building block arrangements, are expected to enhance its functional performance.

Author contributions

Lijuan Liu and Xiaoyang Wang: supervision, writing – review &editing. Shuangyue Shang: writing – original draft, investigation, data curation. Fan Liu and Lei Kang: validation, visualization. Tong Wu and Tianhong Huang: writing – review &editing.

Conflicts of interest

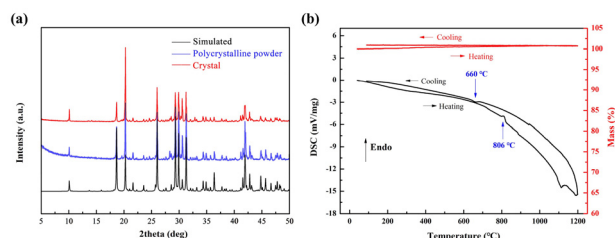There are no conflicts to declare.

Fig. 4 Analysis result of $LiBa_3Al_2B_3O_{11}$ (a) XRD patterns, (b) DSC and TG curves.

Data availability

The data supporting the findings of this study are available within the article and its supplementary information (SI). Supplementary information: EDS analysis, atomic coordinates and equivalent isotropic displacement parameters, anisotropic displacement parameters, bond lengths, bond angles, torsion angles. See DOI: https://doi.org/10.1039/d5dt02373d.

CCDC 2487031 contains the supplementary crystallographic data for this paper.[44]

Acknowledgements

References

1 C. Chen, Y. Wu and R. Li, *Chin. Phys. Lett.*, 1985, **2**, 389–389.
2 C. Chen, Y. Wang, Y. Wu, K. Wu, W. Zeng and L. Yu, *Nature*, 1995, **373**, 322–324.
3 J. M. Tu and D. A. Keszler, *Mater. Res. Bull.*, 1995, **30**, 209–215.
4 C. Chen, Z. Xu, D. Deng, J. Zhang, G. K. L. Wang, B. Wu, N. Ye and D. Tang, *Appl. Phys. Lett.*, 1996, **68**, 2930–2932.
5 M. Mutailipu, K. R. Poeppelmeier and S. Pan, *Chem. Rev.*, 2020, **121**, 1130–1202.
6 G. Peng, N. Ye, Z. Lin, L. Kang, S. Pan, M. Zhang, C. Lin, X. Long, M. Luo and Y. Chen, *Angew. Chem., Int. Ed.*, 2018, **57**, 8968–8972.
7 M. Gao, H. Wu, H. Yu, Z. Hu and Y. Wu, *Sci. China: Chem.*, 2021, **64**, 1184–1191.
8 Z. Chen, K. Zhang, B. Zhang and J. Zhang, *Dalton Trans.*, 2022, **51**, 4097–4103.
9 H. Su, J. Jiao, S. Wang, D. An and M. Zhang, *Dalton Trans.*, 2024, **53**, 932–937.
10 C. Chen, B. Wu, A. Jiang and G. You, *Sci. China, Ser. B: Chem.*, 1985, **28**, 235–243.
11 C. Chen, Y. Wu, A. Jiang, B. Wu, G. You, R. Li and S. Lin, *J. Opt. Soc. Am. B*, 1989, **6**, 616–621.
12 H. Huang, J. Yao, Z. Lin, X. Wang, R. He, W. Yao, N. Zhai and C. Chen, *Angew. Chem., Int. Ed.*, 2011, **50**, 9141–9144.
13 H. Yu, H. Wu, S. Pan, Z. Yang, X. Hou, X. Su, Q. Jing, K. R. Poeppelmeier and J. M. Rondinelli, *J. Am. Chem. Soc.*, 2014, **136**, 1264–1267.
14 S. Zhao, P. Gong, S. Luo, S. Liu, L. Li, M. A. d. Asghar, T. Khan, M. Hong, Z. Lin and J. Luo, *J. Am. Chem. Soc.*, 2015, **137**, 2207–2210.
15 H. Liu, Y. Wang, B. Zhang, Z. Yang and S. Pan, *Chem. Sci.*, 2020, **11**, 694–698.
16 J. Zhou, Y. Liu, H. Wu, H. Yu and Y. Wu, *Angew. Chem., Int. Ed.*, 2020, **59**, 19006–19010.
17 T. Wu, L. Kang, R. Guo, S. Guo, T. Huang, S. Shang, L. Liu and X. Wang, *Inorg. Chem.*, 2025, **64**, 9314–9321.

18 J. Lu, Y. Ou, C. Jin and J. Cheng, *Dalton Trans.*, 2024, **53**, 12034–12042.
19 Y. Ou, X. Zhou, Y. Lan and J. Cheng, *Chin. J. Struct. Chem.*, 2025, **44**, 100708.
20 S. T. Jung, D. Y. Choi, J. K. Kang and S. J. Chung, *J. Cryst. Growth*, 1995, **148**, 207–210.
21 T. Sasaki, Y. Mori and M. Yoshimura, *Opt. Mater.*, 2003, **23**, 343–351.
22 H. Zhang, M. Zhang, S. Pan, Z. Yang, Z. Wang, Q. Bian, X. Hou, H. Yu, F. Zhang, K. Wu, F. Yang, Q. Peng, Z. Xu, K. B. Chang and K. R. Poeppelmeier, *Cryst. Growth Des.*, 2014, **15**, 523–529.
23 J. Zhao, Y. Ma and R. Li, *Appl. Opt.*, 2015, **54**, 9949–9953.
24 A. A. Ballman, *Am. Mineral.*, 1962, **47**, 1380–1383.
25 N. Ye, W. Zeng, B. Wu, X. Huang and C. Chen, *Z. Kristallogr., New Cryst. Struct.*, 1998, **213**, 452.
26 T. Bahti, S. Han, W. Jin, Z. Yang and S. Pan, *Dalton Trans.*, 2020, **50**, 822–825.
27 J. Jiao, M. Zhang and S. Pan, *Angew. Chem., Int. Ed.*, 2023, **62**, e202217037.
28 Q. Li, W. Chen, Y. Lan and J. Cheng, *Chin. J. Struct. Chem.*, 2023, **42**, 100036.
29 N. Ye, W. Zeng, J. Jiang, B. Wu, C. Chen, B. Feng and X. Zhang, *J. Opt. Soc. Am. B*, 2000, **17**, 764–768.
30 Z. Fang, X. Jiang, M. Duan, Z. Hou, C. Tang, M. Xia, L. Liu, Z. Lin, F. Fan and L. Bai, *Chem. – Eur. J.*, 2018, **24**, 7856–7860.
31 Z. Yan, D. Chu, Z. Yang, S. Pan and M. Zhang, *Chem. Commun.*, 2024, **60**, 15047–15050.
32 F. Guo, J. Han, S. Cheng, S. Yu and S. Pan, *Inorg. Chem.*, 2019, **58**, 8237–8244.
33 V. Psycharis, I. A. Kapoutsis and G. D. Chryssikos, *J. Solid State Chem.*, 1999, **142**, 214–219.
34 M. C. Payne, T. A. Arias and J. D. Joannopoulos, *Rev. Mod. Phys.*, 1992, **64**, 1045–1097.
35 S. J. Clark, M. D. Segallii, C. J. Pickardii, P. J. Hasnipiii and M. I. Probertiv, *Z. Kristallogr., Cryst. Struct.*, 2005, **220**, 567–570.
36 J. P. Perdew, K. Burke and M. Ernzerhof, *Phys. Rev. Lett.*, 1998, **77**, 3865–3868.
37 J. Yang, L. Z. Tan and A. M. Rappe, *Phys. Rev. B*, 2017, **97**, 085130.
38 H. Song, N. Wang, X. Jiang, Y. Fu, Y. Li, W. Liu, Z. Lin, J. Yao and G. Zhang, *Inorg. Chem.*, 2019, **58**, 1016–1019.
39 X. Li, D. Chu, W. Jin, Z. Yang, S. Pan and M. Mutailipu, *Inorg. Chem.*, 2022, **61**, 12067–12072.
40 X. Li, D. Chu, H. Qiu, Y. Wu and X. Hou, *Dalton Trans.*, 2023, **52**, 3942–3946.
41 H. Yu, S. Pan, H. Wu, Z. Yang, L. Dong, X. Su, B. Zhang and H. Li, *Cryst. Growth Des.*, 2013, **13**, 3514–3521.
42 Y. Wang, J. Han, J. Huang, Z. Yang and S. Pan, *Inorg. Chem.*, 2020, **59**, 810–817.
43 R. Guo, X. Liu, C. Tao, C. Tang, M. Xia, L. Liu, Z. Lin and X. Wang, *Dalton Trans.*, 2021, **50**, 2138–2142.
44 CCDC 2487031: Experimental Crystal Structure Determination, 2025, DOI: 10.5517/ccdc.csd.cc2pgyty.